

## Supporting Information

# Kinetic modulation-eliminated precursor liquid inclusions in solution method- grown CsPbBr<sub>3</sub> single crystal for radiation detection

Ruichen Bai,<sup>a</sup> Bangzhi Ge,<sup>a</sup> Xin Liu,<sup>a,c</sup> Xinkai Peng,<sup>a</sup> Xin Zhang,<sup>a</sup> Shilin Liu,<sup>a</sup> Menghua Zhu,<sup>a</sup> Chongjian Zhou,<sup>a</sup> Alain Dubois,<sup>b</sup> Wanqi Jie,<sup>a</sup> Yadong Xu<sup>a,\*</sup>

<sup>a</sup> State Key Laboratory of Solidification Processing, and Key Laboratory of Radiation Detection Materials and Devices, Ministry of Industry and Information Technology, Northwestern Polytechnical University, Xi'an 710072, China.

<sup>b</sup> Laboratory of Physical Chemistry – Matter and Radiation, Sorbonne Université, Paris 75005, France.

<sup>c</sup> Aviation Engineering School, Air Force Engineering University, Xi'an 710038, China.

## **Table of contents**

**S1. Relevant information on liquid inclusions**

**S2. Crystal growth principle of CsPbBr<sub>3</sub>**

**S3. Radiation detection performance of control and improve crystals**

## S1. Relevant information on liquid inclusions

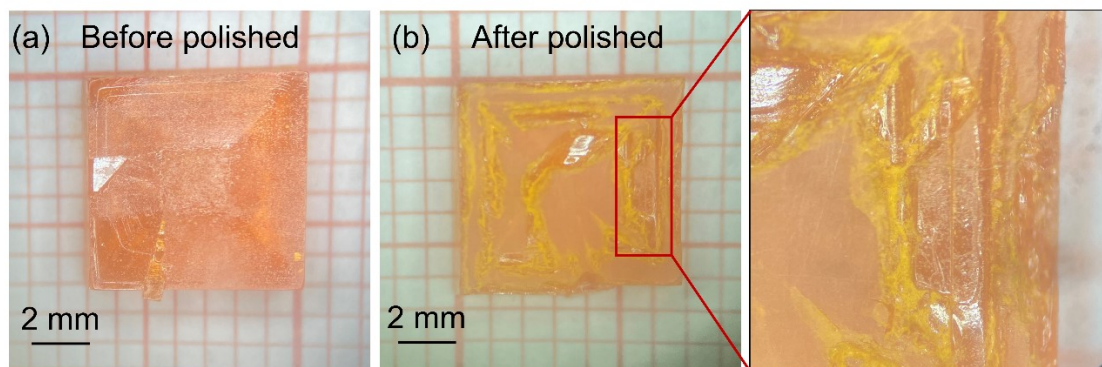


Figure S1. The images of CsPbBr<sub>3</sub> single crystal (a) before polishing and (b) after polishing.

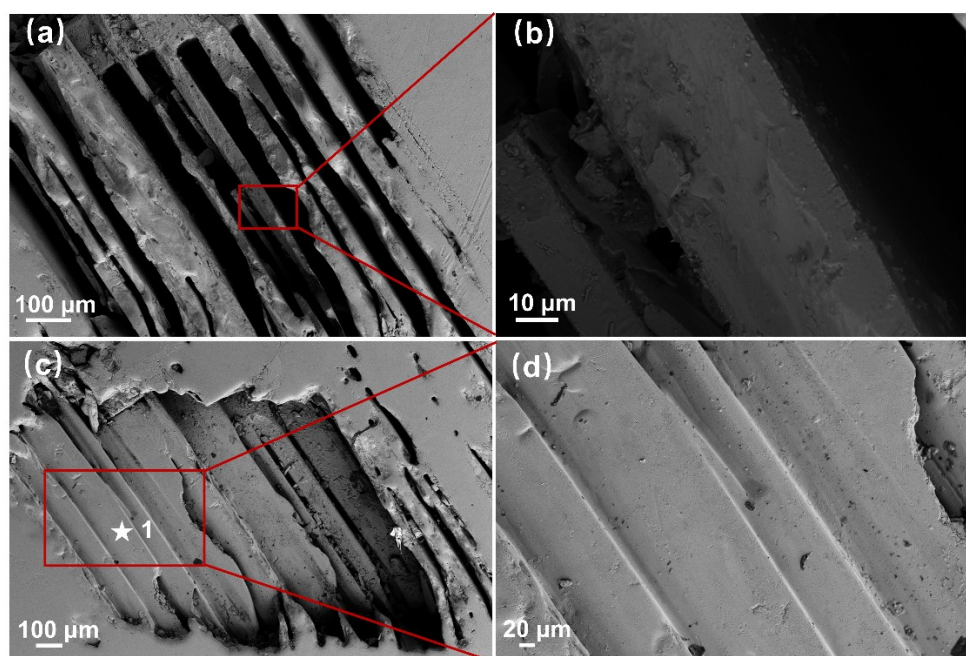


Figure S2. (a) to (d) the detailed SME images of CsPbBr<sub>3</sub> single crystal with liquid inclusions after polishing, the area circled by the red line box is the enlarged area.

Table S1. The ingredients of point 1 in Figure S2(c) were tested by EDS.

Elements	Cs	Pb	Br
Atomic %	18.93	17.61	63.45

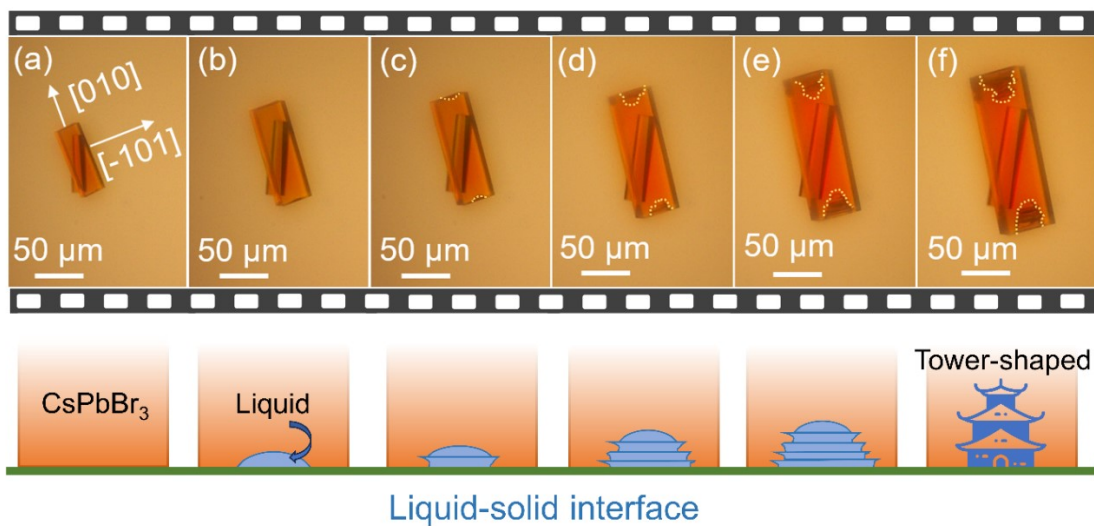


Figure S3. (a) to (f) Images and schematic diagram of  $\text{CsPbBr}_3$  SC obtained in  $60\ ^\circ\text{C}$  from the precursor of 0 min to 15 min. The liquid inclusions area is boxed by the yellow dashed line.

To prove that the inclusions in the crystal are precursor liquid, infrared transmission spectra were utilized. The CsPbBr<sub>3</sub> SC without inclusions and SC with inclusions were chosen. The spectra of these two crystals and precursor were all recorded as shown in Figure S4(a). Noticeably, the spectra for CPB inclusion contain well-defined peaks that are absent for CPB without inclusion. These peaks can be attributed to that observed in the spectra for the precursor. In particular, the peaks at 951 cm<sup>-1</sup> and 1022 cm<sup>-1</sup> are assigned to the C-S and S=O stretch, respectively, and 1392, and 1454 cm<sup>-1</sup> originate from -CH<sub>3</sub> asymmetric<sup>1</sup>, which are all the characteristic peaks of DMSO (the main component of precursor solution). And the peak at 1664 cm<sup>-1</sup> is attributed to the C=O stretch in DMF. Therefore, these peaks have been attributed to the liquid inclusions within the crystal as described in Table S2. Besides, the peaks at 1600 and 3500 cm<sup>-1</sup> are attributed to water vibrational modes, as this experiment was performed under an ambient environment<sup>2</sup>.

To improve the proof, an order CsPbBr<sub>3</sub> SC with liquid inclusions was chosen, and the changes in infrared spectra before and after polishing were compared. Figure S4(b) and (c) show that this SC included liquid inclusions and that after polishing, all the inclusions were eliminated, respectively. From the spectra in Figure S4(b), it is obvious that the spectra exhibit well-defined peaks of precursor before polishing. After removing inclusions, only the peaks of the environment were shown, as CsPbBr<sub>3</sub> is a typical all-inorganic perovskite and does not contain organic functional groups that absorb infrared light.

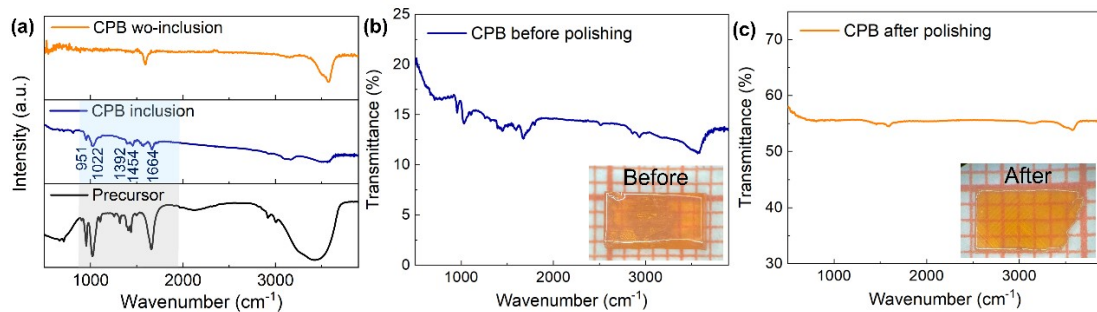


Figure S4. (a) The infrared spectra of CPB wo-inclusion, CPB inclusion, and precursor. (b) to (c) The infrared spectra of CPB (b) before, and (c) after removing inclusions.

Table S2. Origin of infrared absorption peaks

IR peak ( $\text{cm}^{-1}$ )	CPB inclusion peak assignment
951	C-S
1022	S=O
1392	-CH <sub>3</sub> asymmetric
1454	-CH <sub>3</sub> asymmetric
1664	C=O

The crystal growth rate of [-101] and [010] direction was calculated originating from Figure S5, it can be seen that the growth rate exhibited obvious anisotropy, and the growth rate of [010] was three times faster than [-101].

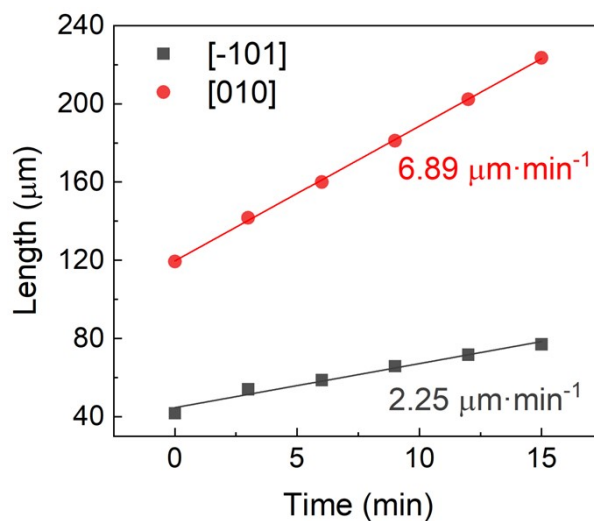


Figure S5. The crystal growth rate of [-101] and [010] direction.

## S2. Crystal growth principle of CsPbBr<sub>3</sub>

The crystal growth rate is controlled by two factors: the transport rate of solute to the growth interface, and the deposition rate of solute at the crystallization interface. There are two boundary layers in the crystallization interface: the growth and diffusion boundary layers. Therefore, the concentration of solute in the solution can be divided into three parameters, the equilibrium solute concentration at the crystallization interface  $\omega_e$ , the interfacial solute concentration between growth boundary layer and diffusion boundary layer  $\omega_i$ , and the solute concentration inside the solution  $\omega_L$ . And  $\omega_e < \omega_i < \omega_L$ , a concentration gradient is exhibited in the crystallization interface, which causes the variation of density and then forms the natural convection.

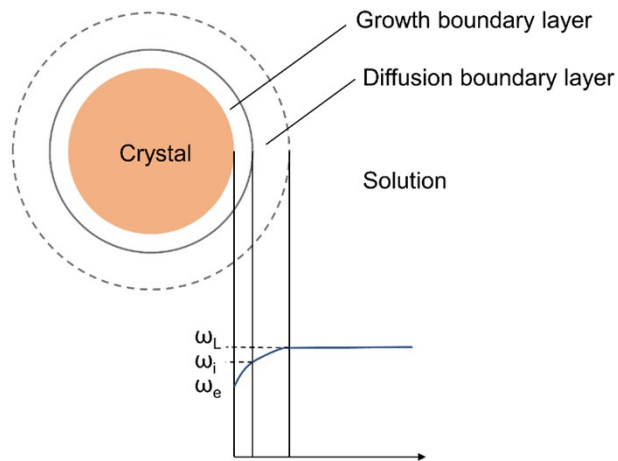


Figure S6. Schematic of the concentration gradient near the crystal growth interface.

The simulation was carried out using COMSOL Multiphysics. The geometric parameters can be seen in Table S3. And the temperature and concentration boundary conditions were set. For the temperature gradient near the CsPbBr<sub>3</sub> SC surface, the latent heat of the crystallization boundary condition was imposed on the growth interface as shown in equation S1:

$$n \cdot (-\kappa \nabla T|_s + \nabla T|_l) = \Lambda Pr_l S f_l n \cdot v_{sl} \quad (S1)$$

Where  $n$  is unit normal vector from crystal to liquid at the growth interface,  $\Lambda = \rho_s / \rho_l$  ( $\rho_s$  and  $\rho_l$  are the density of solid and liquid, respectively),  $S f_l = H_f / c_{p,l} T_{fp,0}$  ( $H_f$  is latent heat of crystallization,  $c_{p,l}$  is the thermal capacity of liquid and  $T_{fp,0}$  is the growth temperature) and  $v_{sl}$  is the crystal growth rate.

For the concentration gradient, the boundary condition is shown in equation S2:

$$\Delta C = 1.66 \frac{\dot{m}}{\rho_0 D} \left( \frac{\rho_0 \nu D^2 x}{g \beta \dot{m}} \right)^{\frac{1}{5}} \quad (S2)$$

Where  $\dot{m}$  is the wall mass flux,  $\rho_0$  is the ambient density at the solution temperature  $T_0$ ,  $D$  is the coefficient of mass diffusivity,  $\nu$  is the kinematic viscosity,  $\beta$  is the coefficient of solutal expansion and  $g$  is the acceleration of gravity.

Table S3. The geometric parameters of COMSOL simulation

	Size	Material
Crystal	d=10 mm h=2 mm	CsPbBr <sub>3</sub>
Growth container	d=100 mm h=150 mm	Glass
Solution	d=100 mm h=150 mm	DMSO

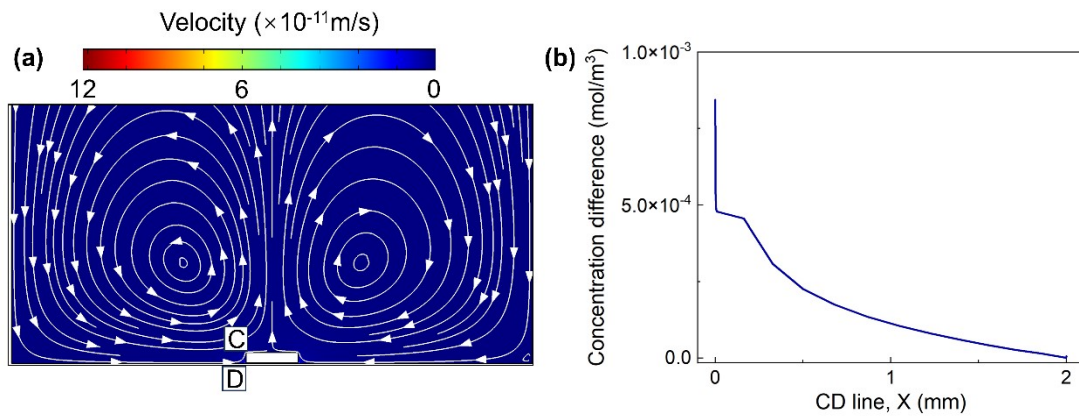


Figure S7. (a) The flow field of natural convection. (b) The concentration distribution of CsPbBr<sub>3</sub>

on the CD line.

The  $\text{CsPbBr}_3$  crystal exhibits a step-like surface as shown in Figure S8. The height of steps is several nanometers scale, which demonstrates that  $\text{CsPbBr}_3$  conforms to a two-dimensional laminar growth mechanism.

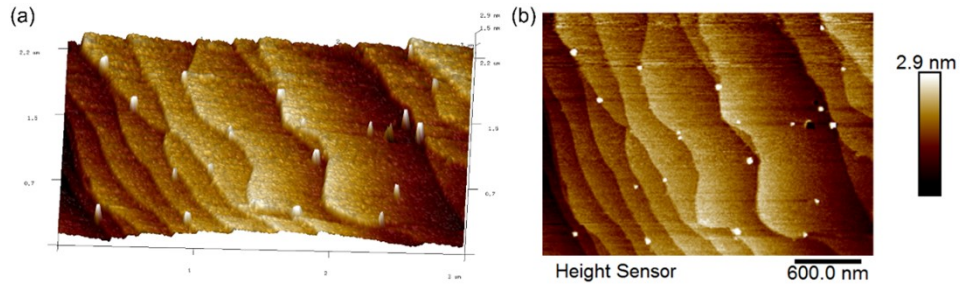


Figure S8. The (a) 3D and (b) 2D typical AFM topography of as-grown  $\text{CsPbBr}_3$  crystal step-like surface.

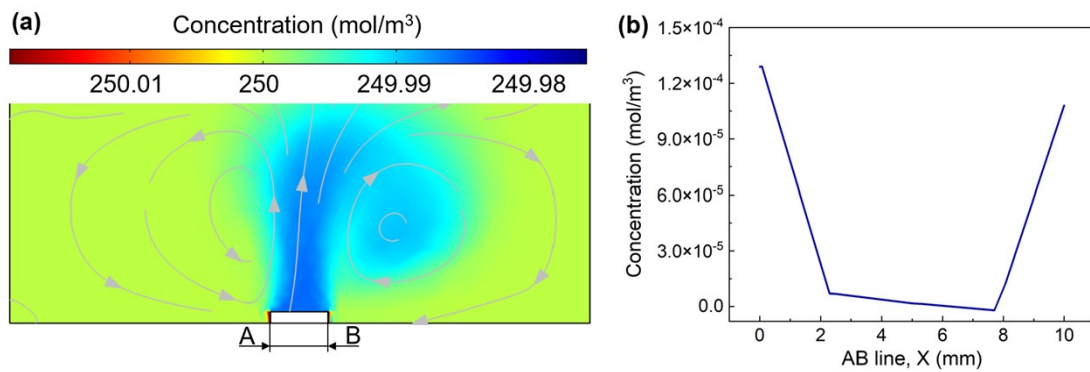


Figure S9. (a) The concentration distribution of Marangni flow. (b) The concentration distribution of AB line with Marangni flow.

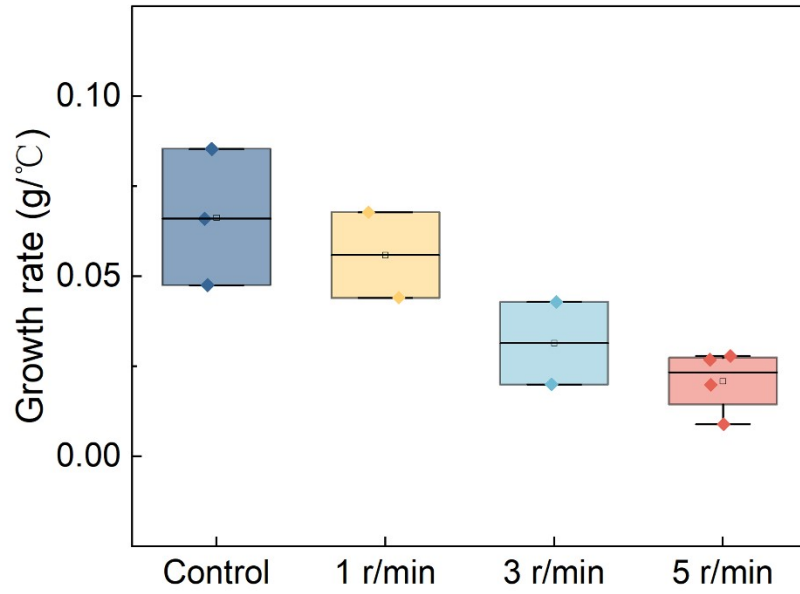


Figure S10. The growth rate of CsPbBr<sub>3</sub> single crystals with different growth methods.

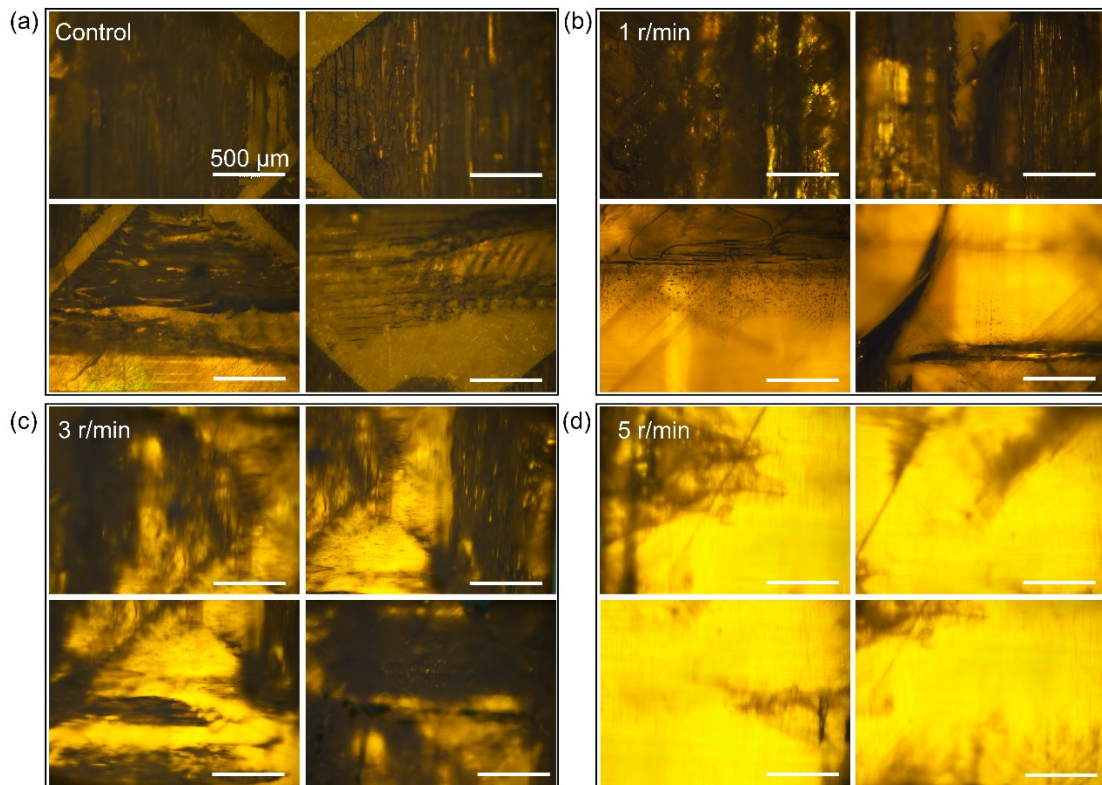


Figure S11. The polarized microscopy images of CsPbBr<sub>3</sub> single crystals grown by (a) normal ITC method. (b) 1 r/min forced convection. (c) 3 r/min forced convection. (d) 5 r/min forced convection. The white ruler represents 500 μm.



### S3 Radiation detection performance of control and improve crystals

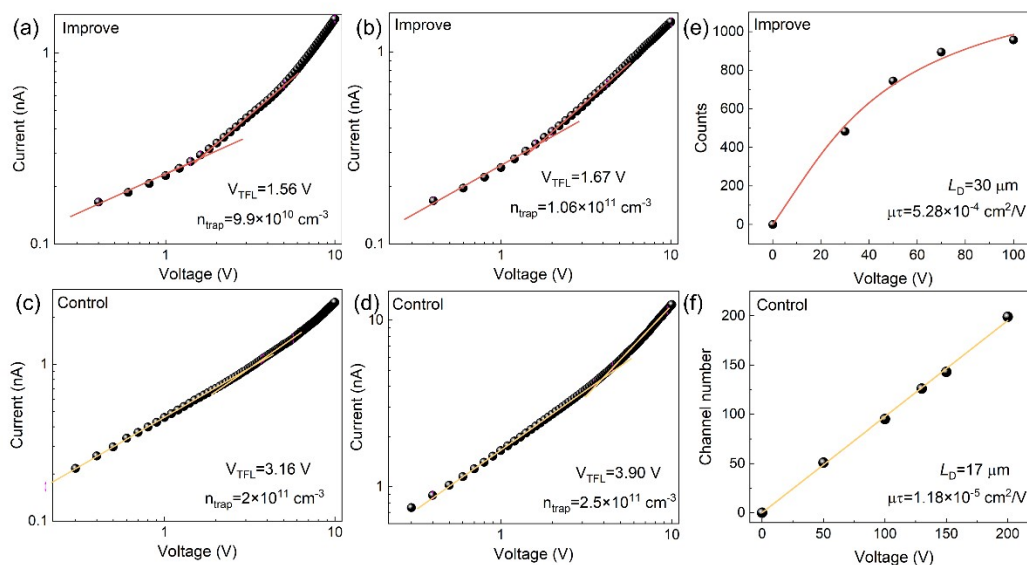


Figure S12. The defect density was measured by the charge limiting current method of (a) and (b) the improved crystals, (c) and (d) the control crystals. The diffusion length of (e) improved crystal and (f) control crystal.

Figure S13(a) and (b) indicate that control SC, which contains liquid inclusions, shows low hole mobility and poor voltage resistance that can only be tested in a voltage lower than 20 V, and the signal-to-noise ratio is poor, resulting in a not obvious full energy peak.

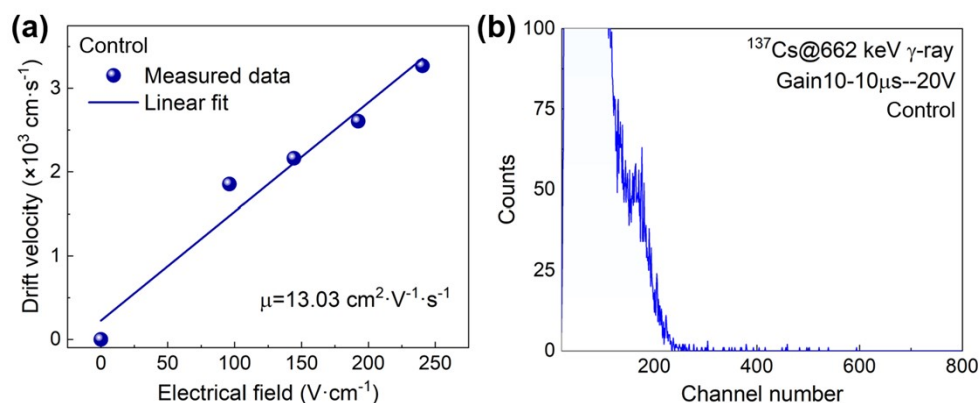


Figure S13. (a) The carrier mobility of control SC. (b) the pulse height spectra of control SC irradiated by  $^{137}\text{Cs}@662\text{ keV}$   $\gamma$ -ray source under -20 V.

Figure S14 shows the pulse height spectra of CsPbBr<sub>3</sub> and CdZnTe detectors with the same crystal size, electrode structure and test parameter. Although the energy resolution displays slightly difference, the spectra show the same details, which the energy resolution variation is attributed to limited carrier transport behaviors of as-grown CsPbBr<sub>3</sub> crystals.

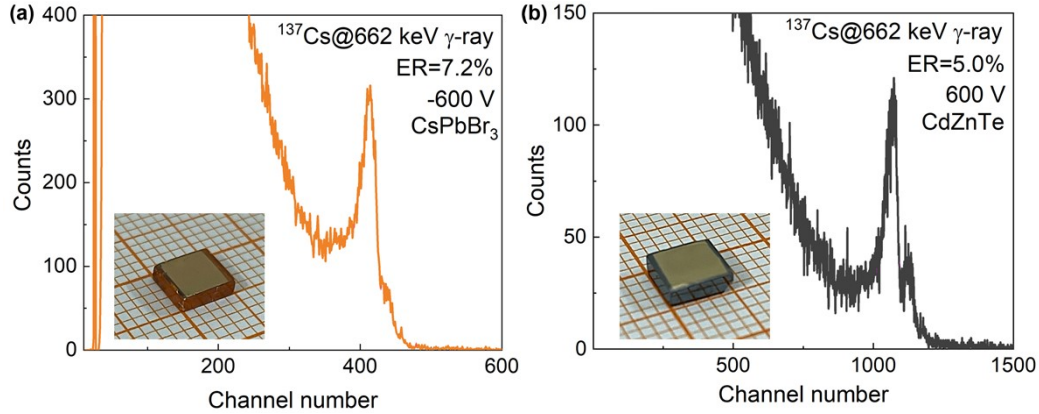


Figure S14. The pulse height spectra of (a) CsPbBr<sub>3</sub> and (b) CdZnTe single crystal irradiated by <sup>137</sup>Cs@662 keV source, the inner pictures are tested crystals with the same electrode and size (5×5×2 mm<sup>3</sup>)

Figure S15 shows the pulse height spectra of control and improved devices irradiated by <sup>241</sup>Am@5.5 MeV alpha particles. The control device can only be tested at a voltage lower than 50 V, but the improved device can be tested from 30 V to 200 V, indicating the CsPbBr<sub>3</sub> crystal without liquid inclusions has a better radiation detection performance.

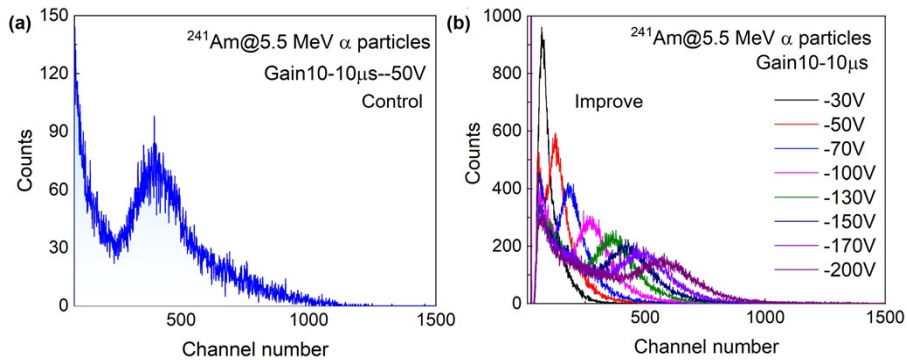


Figure S15. The pulse height spectra of (a) control device irradiated by <sup>241</sup>Am@5.5 MeV alpha particles source under -50 V. (b) improve device irradiated by <sup>241</sup>Am@5.5 MeV alpha particles source from -30 V to -200 V.

## References

1. A. Musiienko, J. Čížek, H. Elhadidy, P. Praus, K. Higgins, B. Dryzhakov, A. Kanak, F. Sureau, J. Pipek, E. Belas, M. Betušiak, M. Brynza, E. Lukosi, B. Hu and M. Ahmadi, *Chemistry of Materials*, 2021, **34**, 297-306.
2. M. Zhang, Z. Zheng, Q. Fu, Z. Chen, J. He, S. Zhang, C. Chen and W. Luo, *Journal of Crystal Growth*, 2018, **484**, 37-42.